



**HAL**  
open science

## Realization of Fully High-Spin State and Strong Ferromagnetism in LaCoO<sub>3</sub> Monolayer

Junhua Liu, Liang Si, Qinghua Zhang, Xiao Wang, Jessica Freese, Grant Harris, Mei Wu, Xinxin Zhang, Ting Lin, Ronny Sutarto, et al.

► **To cite this version:**

Junhua Liu, Liang Si, Qinghua Zhang, Xiao Wang, Jessica Freese, et al.. Realization of Fully High-Spin State and Strong Ferromagnetism in LaCoO<sub>3</sub> Monolayer. *Advanced Functional Materials*, 2024, 10.1002/adfm.202401859 . hal-04599405

**HAL Id: hal-04599405**

**<https://hal.science/hal-04599405v1>**

Submitted on 13 Nov 2024

**HAL** is a multi-disciplinary open access archive for the deposit and dissemination of scientific research documents, whether they are published or not. The documents may come from teaching and research institutions in France or abroad, or from public or private research centers.

L'archive ouverte pluridisciplinaire **HAL**, est destinée au dépôt et à la diffusion de documents scientifiques de niveau recherche, publiés ou non, émanant des établissements d'enseignement et de recherche français ou étrangers, des laboratoires publics ou privés.

# Realization of Fully High-Spin State and Strong Ferromagnetism in LaCoO<sub>3</sub> Monolayer

*Junhua Liu<sup>1,#</sup>, Liang Si<sup>2,3,#</sup>, Qinghua Zhang<sup>4,#</sup>, Xiao Wang<sup>5</sup>, Jessica Freese<sup>6,7</sup>, Grant Harris<sup>6,7</sup>, Mei Wu<sup>8</sup>, Xinxin Zhang<sup>8</sup>, Ting Lin<sup>4,9</sup>, Ronny Sutarto<sup>10</sup>, Javier Herrero-Martin<sup>11</sup>, Charles Guillemard<sup>11</sup>, Manuel Valvidares<sup>11</sup>, Lin Li<sup>1</sup>, Xiaofei Gao<sup>1</sup>, Yaoyao Ji<sup>1</sup>, Zhixiong Deng<sup>1</sup>, Yuhao Hong<sup>1</sup>, Long Wei<sup>1</sup>, Yulin Gan<sup>1</sup>, Lingfei Wang<sup>12</sup>, Guanglei Cheng<sup>13,14</sup>, Peng Gao<sup>8</sup>, Lin Gu<sup>15</sup>, Jiandi Zhang<sup>4</sup>, Zhiwei Hu<sup>5</sup>, Liu Hao Tjeng<sup>5</sup>, Robert J. Green<sup>6,7,\*</sup>, Kai Chen<sup>1,\*</sup>, and Zhaoliang Liao<sup>1,\*</sup>*

<sup>1</sup> National Synchrotron Radiation Laboratory, University of Science and Technology of China, Hefei 230026, China

<sup>2</sup> School of Physics, Northwest University, Xi'an 710127, China

<sup>3</sup> Institute of Solid State Physics, TU Wien, Vienna 1040, Austria

<sup>4</sup> Beijing National Laboratory for Condensed Matter Physics, Institute of Physics, Chinese Academy of Sciences, Beijing 100190, China.

<sup>5</sup> Max Planck Institute for Chemical Physics of Solids, Nöthnitzer Straße 40, Dresden 01187, Germany

<sup>6</sup> Department of Physics and Astronomy and Stewart Blusson Quantum Matter Institute, University of British Columbia, Vancouver, British Columbia V6T 1Z4, Canada

<sup>7</sup> Department of Physics & Engineering Physics, University of Saskatchewan, Saskatoon S7W 0R4, Canada

<sup>8</sup> Electron Microscopy Laboratory, School of Physics and International Center for Quantum Materials, Peking University, Beijing 100871, China

<sup>9</sup> School of Physical Sciences, University of Chinese Academy of Sciences, Beijing 100049, China

<sup>10</sup> Canadian Light Source, Saskatoon, Saskatchewan S7N 2V3, Canada

<sup>11</sup> ALBA Synchrotron Light Source, Cerdanyola del Vallès Barcelona 08290, Spain

<sup>12</sup> Hefei National Research Center for Physical Sciences at Microscale, University of Science and Technology of China, Hefei 230026, China

<sup>13</sup> CAS Key Laboratory of Microscale Magnetic Resonance and School of Physical Sciences, University of Science and Technology of China, Hefei 230026, China

<sup>14</sup> Hefei National Laboratory, Hefei 230088, China

<sup>15</sup> Beijing National Center for Electron Microscopy and Laboratory of Advanced Materials, Department of Materials Science and Engineering, Tsinghua University, Beijing 100084, China

# These authors contributed equally to this work.

\* email: zliao@ustc.edu.cn; kaichen2021@ustc.edu.cn; robert.green@usask.ca

Perovskite  $\text{LaCoO}_3$  has been a subject of extensive and ongoing investigation due to the delicate competition between high-spin (HS) and low-spin (LS) states of  $\text{Co}^{3+}$ . On the other hand, their indistinct free energy boundary poses a significant challenge to annihilate the magnetically/electrically inert LS  $\text{Co}^{3+}$  for yielding fully HS state. Here, we demonstrated electronic transformation from the conventional isovalent mixed HS/LS state ( $\text{La}[\text{Co}_{\text{HS}}^{3+}, \text{Co}_{\text{LS}}^{3+}]\text{O}_3$ ) into an unprecedented aliovalent fully HS state ( $\text{La}[\text{Co}_{\text{HS}}^{3+}, \text{Co}_{\text{HS}}^{2+}]\text{O}_3$ ) in monolayer  $\text{LaCoO}_3$  confined by 5d  $\text{SrIrO}_3$  slabs via atomically constructing  $\text{SrIrO}_3/\text{LaCoO}_3$  superlattices. Excitingly, this emergent fully HS  $\text{La}[\text{Co}_{\text{HS}}^{3+}, \text{Co}_{\text{HS}}^{2+}]\text{O}_3$  monolayer exhibits not only remarkable two-dimensional (2D) ferromagnetism beyond the Mermin-Wagner restriction, but also larger magnetization ( $\sim 1.8\mu_{\text{B}}/\text{Co}$ ) and higher Curie temperature (above 100 K) than that of conventional  $\text{La}[\text{Co}_{\text{HS}}^{3+}, \text{Co}_{\text{LS}}^{3+}]\text{O}_3$  thick film and any previously reported oxide-based monolayer ferromagnets. Furthermore, Ir/Co hybridization driven orbital reconstruction with polarization beyond standard crystal field expectations was observed, which was supported by DFT calculations. Our findings not only expand the electronic phase domains of LCO into fully HS state, but also provide a fresh platform for investigating the 2D magnetic physics under strongly spin-orbit coupled regime and developing new 2D spintronic devices.

**Keywords:**  $\text{LaCoO}_3$  monolayer, spin-state crossover, fully high-spin state, strong 2D ferromagnetism, orbital reconstruction

## 1. Introduction

Spin-state crossover, where the spin state of an ion can be switched by specific stimuli such as temperature <sup>[1]</sup>, strain <sup>[2]</sup>, and light excitation <sup>[3]</sup>, has continuously attracted significant scientific and technological interest owing to remarkable spin-state-controlled properties. Such a phenomenon involves a wide range of fields including magnetics <sup>[2, 4]</sup>, optoelectrics <sup>[3a]</sup>, molecular electronics <sup>[5]</sup>, metalorganic chemistry <sup>[6]</sup> and even geoscience <sup>[7]</sup>, manifesting diverse functionalities <sup>[3a, 8]</sup> such as non-volatile memory, switching, displaying, and energy transduction. 3d cobaltate is an intriguing and representative system with spin-state crossover, where the

prototyped perovskite counterpart,  $\text{LaCoO}_3$  (LCO), has been a subject of increasing attention for over 50 years owing to the high correlation between its magnetism and spin state <sup>[1-2, 4, 9]</sup>. The spin state of  $\text{Co}^{3+}$  mainly depends on the competition between the splitting of the crystal field ( $\Delta_{\text{CF}}$ ) and Hund's exchange ( $J_{\text{H}}$ ) <sup>[1, 2b, 9d, 9e, 10]</sup>. External stimuli can tip the competing balance, leading to a spin-state crossover from the LS  $\text{Co}^{3+}$  ( $t_{2g}^6 e_g^0$ ,  $S = 0$ ) to the mixed state with HS  $\text{Co}^{3+}$  ( $t_{2g}^4 e_g^2$ ,  $S = 2$ ) <sup>[1a, 2b, 9b, 11]</sup>. The LS  $\text{Co}^{3+}$  possessing no electronic/magnetic activity is undesirable <sup>[1a, 12]</sup>, but there is a significant challenge to completely annihilate it thereby leaving only the HS state due to their symbiotic nature caused by the close and ambiguous free energy boundary between HS  $\text{Co}^{3+}$  and LS  $\text{Co}^{3+}$  in LCO <sup>[1a]</sup>. Therefore, as observed in previously reported LCO, regardless of being modified by strain, temperature, or doping/substitution, all  $\text{Co}^{3+}$  exhibited a mixed HS/LS state <sup>[1-2, 4a, 9b, 11a, 13]</sup>. To expand the electronic phase domains and gain insight into the manifestation of LCO with fully HS state, other knobs to effectively suppress the LS  $\text{Co}^{3+}$  are highly desired.

The main fundamental challenge for the realization of fully HS state lies in the six-coordinated  $\text{Co}^{3+}$  in LCO where  $\Delta_{\text{CF}}$  is extremely close to  $J_{\text{H}}$ . In comparison, fully HS  $\text{Co}^{3+}$  has been observed in lower-coordinated cobaltates, such as the  $\text{Sr}_2\text{CoO}_3\text{Cl}_2$  with  $[\text{CoO}_5]$  pyramids <sup>[10]</sup> and  $\text{YBaCo}_4\text{O}_7$  with  $[\text{CoO}_4]$  tetrahedra <sup>[14]</sup>, owing to weaker  $\Delta_{\text{CF}}$  arising from reduced oxygen coordination. Therefore, the question will be, in stoichiometric  $\text{LaCoO}_3$  with the  $[\text{CoO}_6]$  octahedral framework, how to fully suppress LS  $\text{Co}^{3+}$ . Most previous studies about LCO mainly focus on bulk or relatively thick films. Given the highly focused 2D materials, where electron correlation and symmetry breaking are fundamentally different due to the low-dimensional effects and interface interactions, it would be interesting to gain insight into the effect of reduced dimensionality and heterointerface effects on spin-state crossover. Constructing heterostructure allows interweaving various complex interplays from different oxides as well as inversion symmetry breaking <sup>[15]</sup>, providing unprecedented opportunities for tailoring the electronic states of individual components <sup>[16]</sup>. Advanced epitaxial techniques can artificially and precisely

customize the dimensions and interface environment of LCO by introducing specific functional layers, thereby potentially breaking bottleneck of current research on LCO spin-state crossover.

Here, we rationally grew high-quality LCO monolayers by synthesizing superlattices composed of SrIrO<sub>3</sub> (SIO) and LCO to introduce charge transfer, spin-orbit coupling (SOC) and orbital hybridization through the interface as well as the enhanced electron correlations at 2D limit. We are able to fully suppress the LS Co<sup>3+</sup> and therefore to realize an unprecedented fully HS state (La[Co<sub>HS</sub><sup>3+</sup>, Co<sub>HS</sub><sup>2+</sup>]O<sub>3</sub>) in the monolayer limit of LCO in such a superlattice. This emergent species La[Co<sub>HS</sub><sup>3+</sup>, Co<sub>HS</sub><sup>2+</sup>]O<sub>3</sub>, significantly different from the SrTiO<sub>3</sub>-confined LCO monolayer which possesses a mixed HS/LS state and nonmagnetic ground state, displays not only strong 2D ferromagnetism but also orbital reconstruction with large anomalous polarization indicated by our synchrotron spectroscopy together with theoretical calculations. These results suggest a nontrivial 2D HS system with possible multiple coexisting quantum orders, which provides a novel platform for exploring complex interplay and magnetic physics at the 2D limit under strong SOC regime and new applications in 2D electronic devices. Furthermore, our study will provide deep insight into the understanding of spin state transitions and pave a path for engineering the 2D epitaxial magnet for practical application.

## 2. Results

### 2.1. Emergent fully high-spin state in LaCoO<sub>3</sub> monolayer

A series of high-quality [SIO<sub>5</sub>/LCO<sub>*n*</sub>]<sub>10</sub> (S<sub>5</sub>L<sub>*n*</sub>, *n* = 1-10 uc) and [SIO<sub>1</sub>/LCO<sub>1</sub>]<sub>20</sub> (S<sub>1</sub>L<sub>1</sub>)SLs were grown on TiO<sub>2</sub>-terminated SrTiO<sub>3</sub> (STO) (001) substrates. Expected periodic stacking was revealed by high-angle annular dark-field scanning transmission electron microscopy (HAADF-STEM) measurements (see **Figure 1a**). The clear contrast between La (Sr) and Ir (Co) is evidenced, demonstrating abrupt interfaces and coherent growth, which is consistent with results from X-ray diffraction (XRD) and reciprocal space mapping (RSM) (see **Figure S1**). These measurements consistently confirm that a high-quality SIO-confined LCO monolayer was prepared.

X-ray absorption spectra (XAS) measurements were conducted to detect the electronic structure of LCO with varied thickness. The appearance of  $\text{Co}^{2+}$  and the elevation of Ir valence together unravel the charge transfer process <sup>[17]</sup>, i.e.,  $\text{Ir}^{4+} + \text{Co}^{3+} \rightarrow \text{Ir}^{5+} + \text{Co}^{2+}$  (see **Figure S2**). This is in good agreement with the theoretically proposed charge transfer model at perovskite oxide interfaces <sup>[18]</sup>. Such a charge transfer at the interface cooperating with other complex interplays modifies the electronic structure of interfacial area of LCO slabs, eventually giving rise to a fully HS state in the monolayer limit, where the spin state profile can be schematically illustrated as shown in **Figure 1b**. In detail, the contributions of each XAS component were deconvoluted by a linear combination analysis <sup>[12b]</sup>, including HS  $\text{Co}^{2+}$ , HS  $\text{Co}^{3+}$  and LS  $\text{Co}^{3+}$  reference spectra (extracted from ref. <sup>[19]</sup>) as exemplified in **Figure 1c** and **Figure S3**. The fitting results are summarized in **Figure 1d** and **Table S1**, where the percentage of HS  $\text{Co}^{2+}$  increases following an inverse proportional dependence on thickness  $n$ , consistent with the interface charge transfer scenario (see discussion in **SI ,note 4**). In contrast, the percentage of LS  $\text{Co}^{3+}$  shows a monotonic decrease, and thus a significant number of HS Co ions are nominally accumulated with reducing LCO thickness. Ultimately, all the Co ions exhibit the HS state, causing the LCO monolayer ( $\text{S}_5\text{L}_1$  and  $\text{S}_1\text{L}_1$ ) to transform into an emergent monolayer species  $\text{La}[\text{Co}_{\text{HS}}^{3+}, \text{Co}_{\text{HS}}^{2+}]\text{O}_3$ , where their XAS spectra can be well simulated by a linear combination of only HS  $\text{Co}^{2+}$  and HS  $\text{Co}^{3+}$  reference spectra (see **Figure 1c**).

## 2.2 Emergent strong ferromagnetism in $\text{LaCoO}_3$ monolayer

Magnetic characterizations were performed for  $\text{S}_5\text{L}_n$  to elucidate the magnetism of LCO. Normally, the magnetization decays with reducing film thickness due to the “dead layer” effect <sup>[13, 20]</sup> and Mermin-Wagner restriction <sup>[21]</sup> then a ferromagnetic-paramagnetic transition occurs when approaching monolayer thickness as shown by the reference  $[\text{STO}_5/\text{LCO}_1]_{10}$  ( $\text{T}_5\text{L}_1$ ) in **Figure 2a**. With respect to  $\text{S}_5\text{L}_n$  SLs, on the contrary, the ferromagnetism not only surprisingly survives when down to monolayer ( $\text{S}_5\text{L}_1$ ), but is also obviously enhanced compared to thick LCO films. Previous reports have demonstrated that ferromagnetic LCO can induced unsaturated

anomalous Hall effect (AHE) in SIO possessing strong SOC by magneto-proximity effect [17a, 22]. Therefore, the observed unsaturated AHE in S<sub>5</sub>L<sub>1</sub> up to 100 K (see **Figure 2b**) conversely indicates a robust ferromagnetism in the LCO monolayer.

The intrinsic ferromagnetism of ultrathin LCO ( $n = 1-3$ ) was further probed by Co- $L_{2,3}$  X-ray magnetic circular dichroism spectra (XMCD). As shown in **Figure 2c**, the upper panel displays XAS recorded with circularly polarized X-rays with the polarization parallel ( $\mu^+$ ) and antiparallel ( $\mu^-$ ) to the magnetic field direction. The spectral difference ( $\mu^+ - \mu^-$ , namely XMCD) shows finite signals (for raw spectra see **Figure S5**), confirming the ferromagnetism of ultrathin LCO. Their ferromagnetism is collectively contributed by both HS Co<sup>2+</sup> and HS Co<sup>3+</sup>, as shown by comparing the XMCD line-profile with reference spectra [17c]. For instance, the experimental XMCD line-profile in S<sub>5</sub>L<sub>3</sub> can be well reproduced by a linear combination of reference spectra, as shown in **Figure 2d**. The non-monotonic evolution of saturated moment ( $M_{\text{sat}}$ ) with LCO thickness (extracted from **Figure 2a**) is plotted in **Figure 2e**, where a dead-layer-like phenomenon is observed for  $n = 3-10$ , that is, magnetism weakens with reducing thickness. However, the surviving and counterintuitively enhanced magnetization can be observed when thinning LCO to 2D limit ( $n \leq 2$ ), which is much larger than that of thick LCO films [23], verified as well by XMCD in **Figure 2c**.

Element-specific resonant soft X-ray reflectometry (RSXR) [24], an advanced technique to obtain the magnetic as well as the chemical/structural depth profile of the sample with very high precision, was used to investigate global magnetization distribution of S<sub>5</sub>L<sub>1</sub> as illustrated in **Figure 3a**. A strong asymmetry in dichroic circular polarized X-ray spectra was fitted (see **Figure S6**) to yield the periodic magnetization ( $M$ ) profile spatially corresponding to the LCO slabs (see **Figure 3b**), confirming the long-range ferromagnetic order in the LCO monolayer. Notably, the finite magnetic signal under 100 K demonstrates a Curie temperature beyond corresponding thick film (~85 K), which is consistent with the AHE measurement in

**Figure 2b**, confirming the high-ordering temperature of  $\text{La}[\text{Co}_{\text{HS}}^{3+}, \text{Co}_{\text{HS}}^{2+}]\text{O}_3$ .

The enhanced Co moment in  $\text{S}_5\text{L}_1$  can therefore be explained by the crossover from conventional mixed HS/LS states to fully HS state as the thickness of LCO decreases (see **Figure 1d**). The LS  $\text{Co}^{3+}$  exhibits a non-magnetic electron configuration ( $S = 0$ ), while the HS  $\text{Co}^{3+}$  ( $S = 2$ ) possesses a magnetic moment of  $4\mu_{\text{B}}/\text{Co}$ . For conventional thick LCO ( $\text{La}[\text{Co}_{\text{HS}}^{3+}, \text{Co}_{\text{LS}}^{3+}]\text{O}_3$ ), the mixing of LS  $\text{Co}^{3+}$  and HS  $\text{Co}^{3+}$  yields a small nominal moment of  $\sim 1\mu_{\text{B}}/\text{Co}$ . However, for the SIO-confined LCO monolayer, the non-magnetic LS  $\text{Co}^{3+}$  is depleted completely during the charge transfer process, emerging the fully HS monolayer species  $\text{La}[\text{Co}_{\text{HS}}^{3+}, \text{Co}_{\text{HS}}^{2+}]\text{O}_3$  as a combination of HS  $\text{Co}^{3+}$  and HS  $\text{Co}^{2+}$  ( $t_{2g}^5 e_g^2$ ,  $S = 3/2$ ,  $m = 3\mu_{\text{B}}/\text{Co}$ ), as shown in **Figure 1b**. Consequently, it exhibits an enhanced nominal moment ( $\sim 1.8\mu_{\text{B}}/\text{Co}$ ), which is approximately twice as large as that of the single  $\text{LCO}_{30}$  thick film.

### 2.3. Orbital occupancy anomaly and strong polarization

X-ray linear dichroism (XLD, defined as  $I_{E//ab} - I_{E//c}$ ) spectra of the Co- $L_{2,3}$  edge are used to uncover the valence orbital states. As shown in **Figure 4a** (left panel),  $\text{T}_5\text{L}_1$  with electronic structure of  $\text{La}[\text{Co}_{\text{HS}}^{3+}, \text{Co}_{\text{LS}}^{3+}]\text{O}_3$  exhibits an almost zero XLD signal, indicating degenerate Co  $e_g$  and  $t_{2g}$  orbitals instead of the usual tensile strain-driven energy level splitting ( $\text{XLD} < 0$ ). However, for  $\text{S}_5\text{L}_1$ , a significant positive XLD ( $\sim 10\%$ ) was observed (see **Figure 4a**, right panel), indicating a large orbital polarization in the  $\text{La}[\text{Co}_{\text{HS}}^{3+}, \text{Co}_{\text{HS}}^{2+}]\text{O}_3$ . The positive XLD signal demonstrates that the in-plane (IP) orbital energy level is higher than that of the out-of-plane (OOP) orbital, even under tensile strain. We further conducted simulations on the anomaly of the orbital level through multiplet calculations (see **SI, note 7**), which show good agreement with the experimental results, confirming the unforeseen orbital level inversion in the SIO-confined LCO monolayer. Here, might as well define that  $\text{T}_5\text{L}_1$  with degenerate Co  $e_g$  and  $t_{2g}$  orbitals holds an effective tetragonal ratio  $(c/a)_{\text{eff}} \approx 1$ , the preferred OOP population in  $\text{S}_5\text{L}_1$  then suggests that it has  $(c/a)_{\text{eff}} > 1$  and thus the  $c$ -axis of LCO monolayer in  $\text{S}_5\text{L}_1$  could be longer than that in  $\text{T}_5\text{L}_1$ .



To investigate the effective tetragonal ratio further, the lattice profile is probed microscopically by HAADF-STEM. As shown by the profile of the OOP A-A distance (see **Figure 4b** and **Figure S10**), the statistical  $c$ -axis length ( $d_c$ ) of the interfacial LCO layer (3.83 Å) is  $\sim 3\%$  larger than that of the inner LCO layers (3.73 Å). Interface charge transfer from Ir to Co sites, as discussed above, is a possible cause for  $c$ -axis lattice expansion, which has been widely observed in interface charge transfer systems <sup>[17b, 25]</sup>. Furthermore, our DFT calculations (as discussed below) show that strong orbital hybridization between Ir and Co ions reverses Co 3d levels, consistent with the XLD result. That is, interface charge transfer and Ir-Co orbital hybridization could synergistically cause the anomalies of the orbital levels and lattice expansion, leading to a reconstructed orbital state beyond the crystal field expectations.

#### 2.4. Enhanced spin-orbit coupling

Enhanced SOC, affording large magnetocrystalline anisotropy to resist fluctuation for reviving long-range ferromagnetic order, is verified by calculating the Co- $L_{2,3}$  XAS branching ratio <sup>[26]</sup> ( $BR = L_3/L_2$ , for details see **SI, note 8**). As shown in **Figure 4c**, the BR monotonically increases with reducing LCO thickness, demonstrating the stronger BR in the interfacial LCO layer than in the bulk region. This can be interpreted as an increase in the fractions of HS Co<sup>2+</sup> and HS Co<sup>3+</sup> with large BR intuitively, consistent with the spin state profile shown in **Figure 1b**. Notably, BR is also associated with SOC  $\langle \Sigma(l\cdot s) \rangle$  in addition to percentages of HS Co<sup>2+</sup> and HS Co<sup>3+</sup> (Co3d holes  $n_h$ ) according to the formula <sup>[26]</sup>  $(BR-2)/(BR+1) = \langle \Sigma(l\cdot s) \rangle / n_h$ . The significantly enhanced BR cannot be simply described by the increasing fractions of HS Co<sup>2+</sup> and HS Co<sup>3+</sup> with strong SOC. The weighted average value ( $BR^*$ ) of  $S_5L_1$  derived from trivial HS Co<sup>2+</sup> and HS Co<sup>3+</sup> reference spectra <sup>[19]</sup> is shown by the orange five-pointed star in **Figure 4c**, which is much smaller than the experimental BR (red point). The large gap (indicated by the blue arrow) between them strongly suggests that the SOC  $\langle \Sigma(l\cdot s) \rangle$  in the LCO monolayer is additionally enhanced when interfacing with SIO. In contrast, the STO-confined non-magnetic monolayer ( $T_5L_1$ ) shows a BR value (or

SOC) much smaller than that of ferromagnetic S<sub>5</sub>L<sub>1</sub>, indicating that enhanced SOC favors the ferromagnetic order in LCO monolayer.

The orbital-to-spin moment ratio ( $m_{\text{orb}}/m_{\text{s}}$ ) can be calculated from the XMCD sum rules [27]. The  $m_{\text{orb}}/m_{\text{s}}$  systematically increased with thinning LCO (see **Figure 4d** and **Table S2**), and its maximum ( $\sim 0.4$ ) is observed in both S<sub>1</sub>L<sub>1</sub> and S<sub>5</sub>L<sub>1</sub>. Given the total saturated moment of  $1.8\mu_{\text{B}}/\text{Co}$  in S<sub>5</sub>L<sub>1</sub> (at 2 K), the unquenched orbital moment can be estimated to be  $m_{\text{orb}} = 0.51\mu_{\text{B}}/\text{Co}$ . Furthermore, the XMCD results show that S<sub>1</sub>L<sub>1</sub> possesses more HS Co<sup>3+</sup> (less HS Co<sup>2+</sup>) participation in the magnetic contribution than S<sub>5</sub>L<sub>1</sub> yet has a similar  $m_{\text{orb}}/m_{\text{s}}$  as S<sub>5</sub>L<sub>1</sub>, indicating that the HS Co<sup>3+</sup> possesses a comparable  $m_{\text{orb}}/m_{\text{s}}$  as HS Co<sup>2+</sup>, or  $m_{\text{orb}}/m_{\text{s}}$  of both HS Co<sup>2+</sup> and HS Co<sup>3+</sup> is enhanced in the ferromagnetic LCO monolayer, consistent with the additionally enhanced SOC as discussed above.

## 2.5. DFT+U Calculations

DFT+U calculations were employed to investigate the electronic and magnetic properties of the LCO monolayers. Our calculations show that the ground state of the STO-strained LCO single film is ferromagnetic, while the ferromagnetic order collapses when LCO is confined by STO to monolayer thickness (T<sub>5</sub>L<sub>1</sub>, see **Figure S13**). This finding is foreseeable and consistent with previous reports [13]. For the SIO-confined LCO monolayer (S<sub>5</sub>L<sub>1</sub>), strong interface electron transfer is observed from Ir to Co sites, consistent with our experimental results and previous reports [17a, 17b, 18]. We further attempt to understand the coexistence of HS Co<sup>3+</sup> and HS Co<sup>2+</sup>, where three possible states can be derived as shown in **Figure S14**. **Figures 5a** and **5b** show the total and partial DOS of Co ions in S<sub>5</sub>L<sub>1</sub> in the ground state (right panel in **Figure 5c**). Apparently asymmetric spin subbands are observed for both HS Co<sup>3+</sup> and HS Co<sup>2+</sup>, demonstrating ferromagnetism in the LCO monolayer.

We further observed strong hybridization between the localized Co3d orbital and itinerant Ir5d orbital. Generally, SIO (LCO) grown on STO suffers from compressive (tensile) strain, which causes the t<sub>2g</sub> electrons in SIO (LCO) to tend to occupy

out-of-plane  $d_{xz}/d_{yz}$  (in-plane  $d_{xy}$ ) orbitals. The strong orbital hybridization and charge transfer between Ir and Co ions drives the reconstruction of the Co3d orbital, resulting in bonding  $d_{xz}/d_{yz}$  and  $d_z^2$  orbitals with reduced energy below the in-plane  $d_{xy}$  and  $d_x^2 - y^2$  orbitals (see **Figure 5c**), which is consistent with the XLD results. In addition, antibonding  $d_{xz}/d_{yz}$  states emerge near the Fermi level, which significantly narrows the band gap compared with STO/LCO SLs and reveals half-metal features. Intriguingly, our calculations further indicate orbital order and charge order in the ground state of  $S_5L_1$ , which needs to be further experimentally confirmed.

### 3. Discussion and conclusions

The introduction of electron-rich 5d SIO is vital for realizing the fully HS state and thus strong ferromagnetism in LCO monolayer. First, at the LCO/SIO interface, charge-transfer-induced  $Ir^{5+}$  can pull harder on  $O^{2-}$  compared with  $Co^{3+}$  [12b, 28], causing  $O^{2-}$  away from  $Co^{3+}$  ions thus anomalously elongates the  $c$ -axis, as revealed by the HAADF-STEM results (see **Figure 4b**). Together with in-plane tensile strain, the  $\Delta_{CF}$  can be reduced significantly thereby annihilating LS  $Co^{3+}$  and promoting fully HS state. Second, the reduction in dimensionality enhances the strength of electron correlations, leading to a preferred population at different orbitals in order to minimize the Coulomb repulsion through spatial avoidance thereby favoring HS state [29]. For instance, the non-charge-transferred LCO monolayer  $T_5L_1$  exhibits more (less) HS  $Co^{3+}$  (LS  $Co^{3+}$ ) than the bulk-like LCO counterparts  $S_5L_{10}$  (see **Table S1**). In addition, SOC may also play a role in stabilizing HS state. LS  $Co^{3+}$  ions exhibit weak SOC, which makes them unfavorable for survival in the presence of SIO slabs with strong SOC.

The pronounced enhancement of SOC in LCO monolayer, on the one hand, could be attributed to the proximity effect from SIO with strong SOC [30]; and on the other hand, it can be contributed by Rashba-like effect from the interfacial built-in electric field ( $E: SIO^+ \rightarrow LCO^-$ ) due to charge transfer. Notably, the enhancement of SOC plays an essential role in stabilizing the ferromagnetism of LCO monolayer by supplying

magnetic anisotropy so as counteracting Mermin-Wagner restriction <sup>[21b]</sup>, as indicated by some 2D van der Waals ferromagnets <sup>[21a, 31]</sup>. The ferromagnetic order in such an aliovalent HS Co<sup>2+</sup>/HS Co<sup>3+</sup> system is governed by the double-exchange interaction. Different from the manganates where ferromagnetism is mediated by  $e_g$  orbital through "head-to-head"  $\sigma$  overlap <sup>[32]</sup>, the exchange in La[Co<sub>HS</sub><sup>3+</sup>, Co<sub>HS</sub><sup>2+</sup>]O<sub>3</sub> is mediated by  $t_{2g}$  orbital through Co3d-O2p "shoulder-to-shoulder"  $\pi$  ( $\pi_{d-p}$ ) overlap (see the right panel in **Figure 5c**), similar to the case in hole-doped counterpart La<sub>0.7</sub>Sr<sub>0.3</sub>CoO<sub>3</sub> film <sup>[11a]</sup>.

In summary, we demonstrated that, by constructing 3d/5d heterointerfaces, an unprecedented fully HS state was realized in SIO-confined LCO monolayer. Such an emergent spin state synergistically exists with ferromagnetic order and large orbital polarization, sharply contrasting with the trivial STO-confined LCO monolayer. Attributed to the strong SOC and the enhanced exchange interactions caused by valence mixture, the ferromagnetic order survives above 100 K, showing the highest Curie temperature and largest atomic moment ( $\sim 1.8\mu_B/\text{Co}$ ) compared to any previous oxide-based 2D ferromagnets. The orbital reconstruction, driven by interfacial 3d-5d hybridization, exhibits a reversal of the Co3d levels that goes beyond the expectations derived from crystal field physics. The strong SOC, which collaborates with the broken inversion symmetry at interface, likely provides significant antisymmetric exchange coupling effect such as Dzyaloshinskii-Moriya interaction <sup>[33]</sup>, thereby possibly exhibiting a promising host for searching for 2D skyrmion-like spin texture <sup>[34]</sup>. Besides, such a stacking of heavy-metal layer/2D ferromagnet heterostructure (SIO/LCO) can serve as the base material of potential ultra-compact devices for spintronic applications <sup>[35]</sup>.

#### 4. Experimental Section/Methods

*Sample growth:* The SIO/LCO and LCO/STO superlattices were grown on TiO<sub>2</sub>-terminated SrTiO<sub>3</sub> (001) substrates by Laser molecular beam epitaxy (Laser-MBE) assisted by *in-situ* reflection high energy electron diffraction (RHEED), operating at 248 nm. The TiO<sub>2</sub>-terminated SrTiO<sub>3</sub> (001) substrate were obtained by

etching with standard buffered oxide etch (BOE) solution and subsequent annealing at 950 °C for 90 min. Laser fluence and repetition rate during growth were 1.1 J/cm<sup>2</sup> and 4 Hz, respectively. Typical substrate temperature was 660 °C and the oxygen partial pressure was 0.15 mbar. The thickness of each sub-layer was precisely monitored by *in-situ* RHEED. A series of superlattices  $S_mL_n$  with  $m = 1, 5$  uc and  $n = 1-10$  uc were prepared using two-target growth alternating LaCoO<sub>3</sub> and SrIrO<sub>3</sub>.  $S_1L_1$  possesses 20 periodic repetitions in order to facilitate XRD measurements, while the other samples all keep 10 repetitions. Superlattices for structure characterization and magnetization measurement were capped by ~ 4 nm amorphous STO (*a*-STO) in order to protect the periodic superlattices structure. The SIO/LCO (STO/LCO) superlattices for synchrotron X-ray experiment were terminated by additional crystalline SIO (STO) layer for preventing phase decomposition of LCO to be probed.

*Structural characterization:* Surface morphology was recorded by atomic force microscope (AFM). X-ray diffraction (XRD), reflectivity (XRR) and reciprocal space mapping (RSM) measurements were carried out for characterizing the crystal structure, crystallinity and orientation by using a high resolution X-ray diffractometer (Malvern PANalytical). The XRR data were fitted using the chemical depth profiles by GenX software. The microscopic chemical configuration of superlattices was measured by High-angle annular dark-field scanning transmission electron microscopy (HAADF-STEM). The cross-section specimens of  $S_5L_1$  and  $S_1L_1$  were prepared by mechanical grinding then Ar ion beam milling. The atom positions were determined by fitting with 2D Gaussian peaks using a MATLAB code.<sup>[36]</sup> Then the lattice parameter along *c*-axis ( $d_c$ ) can be estimated as the distance between two neighboring A-site atoms (including La-La, La-Sr and Sr-Sr pairs).

*Magnetization and transport characterization:* Both in-plane and out-of-plane field-dependent magnetization were measured by MPMS 3 (Quantum Design), where the sample was loaded by a standard quartz paddle holder. The actual sample magnetization was acquired by subtracting a linear diamagnetic contribution from the STO substrate. Electrical transport measurements were based on the van der Pauw

method using a PPMS-9T (Quantum Design). The Hall signals are “odd” with respect to the applied field, thus they were calculated as  $R_{xy} = (R_{xy}^{raw}(H) - R_{xy}^{raw}(-H))/2$ . Then, the anomalous Hall effect ( $R_{AHE}$ ) could be obtained by deducting the ordinary Hall effect ( $R_{OHE}$ ), i.e.,  $R_{AHE} = R_{xy} - R_{OHE}$ . Due to the field is insufficient to saturate the Hall hysteresis, conventionally sweeping field at a fixed temperature can only produce an undesired minor Hall hysteresis without saturating the sample and quenching the magnetic domains. In order to trace the correct major Hall hysteresis, one has to quench the domains by thermal heating and cooling, where the detailed measurement see ref. [37].

*Synchrotron X-ray experiment:* X-ray absorption spectroscopy (XAS) and magnetic circular dichroism (XMCD) were conducted at the Boreas beamline of ALBA Synchrotron Light Source<sup>[38]</sup>. The measurements were performed under 6 T at 10 K, with the incoming X-ray and magnetic field perpendicular to the sample plane. Resonant soft X-ray reflectometry (RSXR) spectra were measured at the REIXS beamline of the Canadian Light Source (CLS) with a magnetic field (0.6 T) parallel to the sample plane. The samples were aligned with their surface normal in the scattering plane and measured at 20 K and 100 K. The measurements were carried out in the specular reflection geometry with several non-resonant photon energies as well as energies at the Co- $L_{2,3}$  resonance ( $\sim 765$ -805 eV). The X-ray linear dichroism (XLD) of  $S_5L_1$  was measured at the CLS as well as Hefei Light Source, and XLD of  $T_5L_1$  was measured at Hefei Light Source. For XLD measurement, the incident X-ray was at  $90^\circ$  and  $25^\circ$  angles to the sample plane at Hefei Light Source, and the X-ray was at the grazing angle of  $25^\circ$  at the CLS where measuring by varying the linear polarization. All X-ray absorption experiments data was recorded using a mode of total electron yield. X-ray photoelectron spectroscopy (XPS) were measured by an in-house photoelectron spectrometer (Thermo Scientific ESCALAB 250Xi) with ultimate vacuum pressure of  $5 \times 10^{-10}$  mbar. The Al  $K\alpha$  X-ray monochromator was operated with an anode power of 150 W.

*DFT Calculations:* We employed the DFT+U method<sup>[39]</sup> to investigate the electronic

and magnetic properties of  $(\text{SrIrO}_3)_5/(\text{LaCoO}_3)_1$  and  $(\text{SrTiO}_3)_5/(\text{LaCoO}_3)_1$  superlattices using GGA-PBE correlation-exchange functional<sup>[40]</sup>. All first-principles calculations were performed within the Vienna Ab Initio Simulation Package (VASP) and Wien2k codes. More details see **SI, note 10**.

### **Supporting Information**

Supporting Information is available from the Wiley Online Library or from the author.

### **Acknowledgments**

We thank Dr. Xuguang Liu from Instruments Center for Physical Science, USTC for assistance in macroscopic magnetic measurements. This work was supported by the National Key R&D Program of China (No. 2022YFA1403000) and the National Natural Science Foundation of China (Nos. 52272095 and 11974325). K.C. acknowledges support from the Collaborative Innovation Program of Hefei Science Center, CAS (No. CX2310000177), the National Natural Science Foundation of China (No. 12275272) and the Fundamental Research Funds for the Central Universities (Nos. wk2310000104 and wk2310000106). Q.Z. acknowledges support from the National Natural Science Foundation of China (Nos. 52072400, 52025025 and 51991344), the Beijing Natural Science Foundation (No. Z190010) and the National Key R&D Program of China (No. 2019YFA0308500). Part of the research described in this paper was performed at the Canadian Light Source, a national research facility of the University of Saskatchewan, which is supported by the Canada Foundation for Innovation (CFI), the Natural Sciences and Engineering Research Council (NSERC), the National Research Council Canada (NRC), the Canadian Institutes of Health Research (CIHR), the Government of Saskatchewan, and the University of Saskatchewan. We would like to thank the BOREAS beamline of the ALBA Synchrotron Light Facility with the collaboration of ALBA staff (beamtime proposal 2022025648) and MCD-A and MCD-B (Soochow Beamline for Energy Materials) beamlines of NSRL for the synchrotron beamtime.

### **Conflict of Interest**

The authors declare no competing interests.

### **Author contributions**

Z.L., K.C. and R.J.G. conceived the project. J.H. performed the sample preparation, structure and morphology characterization and magnetic measurements. Q.Z., T.L., M.W., X.Z., P.G. and L.G. performed the HAADF-STEM measurements and atomic position fitting. J.L., K.C., R.J.G., L.H.T., Z.H., X.W., J.F., G.H., R.S., J.H.-M., C.G. and M.V. conducted the synchrotron X-ray experiments and analyzed the results. L.S. performed the DFT+U calculations. G.C. directed the AFM measurement. J.L., L.S., J.Z., Z.L., K.C. and R.J.G. wrote the paper. All authors contributed to the data discussions and analysis.

**Data and materials availability:** The data that support the findings of this study are available from the corresponding author upon reasonable request.



## References

- [1] a)M. W. Haverkort, Z. Hu, J. C. Cezar, T. Burnus, H. Hartmann, M. Reuther, C. Zobel, T. Lorenz, A. Tanaka, N. B. Brookes, H. H. Hsieh, H. J. Lin, C. T. Chen, L. H. Tjeng, *Phys. Rev. Lett.* **2006**, 97, 176405; b)D. Takegami, A. Tanaka, S. Agrestini, Z. Hu, J. Weinen, M. Rotter, C. Schüßler-Langeheine, T. Willers, T. C. Koethe, T. Lorenz, Y. F. Liao, K. D. Tsuei, H. J. Lin, C. T. Chen, L. H. Tjeng, *Phys. Rev. X* **2023**, 13, 011037.
- [2] a)D. Fuchs, C. Pinta, T. Schwarz, P. Schweiss, P. Nagel, S. Schuppler, R. Schneider, M. Merz, G. Roth, H. v. Löhneysen, *Phys. Rev. B* **2007**, 75, 144402; b)E.-J. Guo, R. Desautels, D. Lee, M. A. Roldan, Z. Liao, T. Charlton, H. Ambaye, J. Molaison, R. Boehler, D. Keavney, A. Herklotz, T. Z. Ward, H. N. Lee, M. R. Fitzsimmons, *Phys. Rev. Lett.* **2019**, 122, 187202.
- [3] a)S.-Q. Su, S.-Q. Wu, Y.-B. Huang, W.-H. Xu, K.-G. Gao, A. Okazawa, H. Okajima, A. Sakamoto, S. Kanegawa, O. Sato, *Angew. Chem., Int. Ed.* **2022**, 61, e202208771; b)M. Nadeem, J. Cruddas, G. Ruzzi, B. J. Powell, *J. Am. Chem. Soc.* **2022**, 144, 9138.
- [4] a)J. W. Freeland, J. X. Ma, J. Shi, *Appl. Phys. Lett.* **2008**, 93, 212501; b)S. Chikara, J. Gu, X. G. Zhang, H.-P. Cheng, N. Smythe, J. Singleton, B. Scott, E. Krenkel, J. Eckert, V. S. Zapf, *Nat. Commun.* **2019**, 10, 4043.
- [5] E. Ruiz, *Phys. Chem. Chem. Phys.* **2014**, 16, 14.
- [6] A. Köbke, F. Gutzeit, F. Röhricht, A. Schlimm, J. Grunwald, F. Tuzcek, M. Studniarek, D. Longo, F. Choueikani, E. Otero, P. Ohresser, S. Rohlf, S. Johannsen, F. Diekmann, K. Rossnagel, A. Weismann, T. Jasper-Toennies, C. Näther, R. Herges, R. Berndt, M. Gruber, *Nat. Nanotechnol.* **2020**, 15, 18.
- [7] J.-F. Lin, V. V. Struzhkin, S. D. Jacobsen, M. Y. Hu, P. Chow, J. Kung, H. Liu, H.-k. Mao, R. J. Hemley, *Nature* **2005**, 436, 377.
- [8] a)K. S. Kumar, M. Ruben, *Angew. Chem., Int. Ed.* **2021**, 60, 7502; b)O. Kahn, C. J. Martinez, *Science* **1998**, 279, 44; c)S. P. Vallone, A. N. Tantillo, A. M. dos Santos, J. J. Molaison, R. Kulmaczewski, A. Chapoy, P. Ahmadi, M. A. Halcrow, K. G. Sandeman, *Adv. Mater.* **2019**, 31, 1807334.
- [9] a)W. S. Choi, J.-H. Kwon, H. Jeon, J. E. Hamann-Borrero, A. Radi, S. Macke, R. Sutarto, F. He, G. A. Sawatzky, V. Hinkov, M. Kim, H. N. Lee, *Nano Lett.* **2012**, 12, 4966; b)V. Chaturvedi, S. Ghosh, D. Gautreau, W. M. Postiglione, J. E. Dewey, P. Quarterman, P. P. Balakrishnan, B. J. Kirby, H. Zhou, H. Cheng, A. Huon, T. Charlton, M. R. Fitzsimmons, C. Korostynski, A. Jacobson, L. Figari, J. G. Barriocanal, T. Birol, K. A. Mkhoyan, C. Leighton, *Nat. Commun.* **2022**, 13, 7774; c)P. M. Raccah, J. B. Goodenough, *Phys. Rev.* **1967**, 155, 932; d)M. A. Korotin, S. Y. Ezhov, I. V. Solovyev, V. I. Anisimov, D. I. Khomskii, G. A. Sawatzky, *Phys. Rev. B* **1996**, 54, 5309; e)Y. Yokoyama, Y. Yamasaki, M. Taguchi, Y. Hirata, K. Takubo, J. Miyawaki, Y. Harada, D. Asakura, J. Fujioka, M. Nakamura, H. Daimon, M. Kawasaki, Y. Tokura, H. Wadati, *Phys. Rev. Lett.* **2018**, 120, 206402.
- [10] Z. Hu, H. Wu, M. W. Haverkort, H. H. Hsieh, H. J. Lin, T. Lorenz, J. Baier, A. Reichl, I. Bonn, C. Felser, A. Tanaka, C. T. Chen, L. H. Tjeng, *Phys. Rev. Lett.* **2004**, 92, 207402.
- [11] a)D. Fuchs, M. Merz, P. Nagel, R. Schneider, S. Schuppler, H. von Löhneysen, *Phys. Rev. Lett.* **2013**, 111, 257203; b)J. S. Zhou, J. Q. Yan, J. B. Goodenough, *Phys. Rev. B* **2005**, 71, 220103.
- [12] a)X.-j. Li, B.-T. Wang, W. Yin, *J. Magn. Magn. Mater.* **2022**, 555, 169318; b)C. F. Chang, Z. Hu, H. Wu, T. Burnus, N. Hollmann, M. Benomar, T. Lorenz, A. Tanaka, H. J. Lin, H. H. Hsieh, C. T. Chen, L. H. Tjeng, *Phys. Rev. Lett.* **2009**, 102, 116401; c)S. Li, J. Wang, Q. Zhang, M. A. Roldan, L. Shan, Q.

- Jin, S. Chen, Z. Wu, C. Wang, C. Ge, M. He, H. Guo, L. Gu, K.-j. Jin, E.-J. Guo, *Phys. Rev. Mater.* **2019**, 3, 114409.
- [13] D. Meng, H. Guo, Z. Cui, C. Ma, J. Zhao, J. Lu, H. Xu, Z. Wang, X. Hu, Z. Fu, R. Peng, J. Guo, X. Zhai, G. J. Brown, R. Knize, Y. Lu, *Proc. Natl. Acad. Sci. U. S. A.* **2018**, 115, 2873.
- [14] N. Hollmann, Z. Hu, M. Valldor, A. Maignan, A. Tanaka, H. H. Hsieh, H. J. Lin, C. T. Chen, L. H. Tjeng, *Phys. Rev. B* **2009**, 80, 085111.
- [15] R. Ramesh, D. G. Schlom, *Nat. Rev. Mater.* **2019**, 4, 257.
- [16] H. Y. Hwang, Y. Iwasa, M. Kawasaki, B. Keimer, N. Nagaosa, Y. Tokura, *Nat. Mater.* **2012**, 11, 103.
- [17] a)J. Liu, X. Zhang, Y. Ji, X. Gao, J. Wu, M. Zhang, L. Li, X. Liu, W. Yan, T. Yao, Y. Yin, L. Wang, H. Guo, G. Cheng, Z. Wang, P. Gao, Y. Wang, K. Chen, Z. Liao, *J. Phys. Chem. Lett.* **2022**, 13, 11946; b)X. Liu, M. Kotiuga, H. S. Kim, A. T. N'Diaye, Y. Choi, Q. Zhang, Y. Cao, M. Kareev, F. Wen, B. Pal, J. W. Freeland, L. Gu, D. Haskel, P. Shafer, E. Arenholz, K. Haule, D. Vanderbilt, K. M. Rabe, J. Chakhalian, *Proc. Natl. Acad. Sci. U. S. A.* **2019**, 116, 19863; c)S. Agrestini, K. Chen, C. Y. Kuo, L. Zhao, H. J. Lin, C. T. Chen, A. Rogalev, P. Ohresser, T. S. Chan, S. C. Weng, G. Auffermann, A. Völzke, A. C. Komarek, K. Yamaura, M. W. Haverkort, Z. Hu, L. H. Tjeng, *Phys. Rev. B* **2019**, 100, 014443.
- [18] Z. Zhong, P. Hansmann, *Phys. Rev. X* **2017**, 7, 011023.
- [19] S. C. Haw, Z. Hu, H. J. Lin, J. M. Lee, H. Ishii, N. Hiraoka, A. Meléndez-Sans, A. C. Komarek, L. H. Tjeng, K. Chen, C. Luo, F. Radu, C. T. Chen, J.-M. Chen, *J. Alloys Compd.* **2021**, 862, 158050.
- [20] a)M. Huijben, L. W. Martin, Y. H. Chu, M. B. Holcomb, P. Yu, G. Rijnders, D. H. A. Blank, R. Ramesh, *Phys. Rev. B* **2008**, 78, 094413; b)J. Xia, W. Siemons, G. Koster, M. R. Beasley, A. Kapitulnik, *Phys. Rev. B* **2009**, 79, 140407(R).
- [21] a)C. Gong, X. Zhang, *Science* **2019**, 363, eaav4450; b)N. D. Mermin, H. Wagner, *Phys. Rev. Lett.* **1966**, 17, 1133.
- [22] S. Rom, S. Baidya, S. Bhattacharjee, T. Saha-Dasgupta, *Appl. Phys. Lett.* **2023**, 122, 021602.
- [23] D. Shin, S. Yoon, S. Song, S. Park, H. N. Lee, W. S. Choi, *Adv. Mater. Interfaces* **2022**, 9, 2200433.
- [24] Z. Liao, M. Huijben, Z. Zhong, N. Gauquelin, S. Macke, R. J. Green, S. Van Aert, J. Verbeeck, G. Van Tendeloo, K. Held, G. A. Sawatzky, G. Koster, G. Rijnders, *Nat. Mater.* **2016**, 15, 425.
- [25] S. Lee, A. T. Lee, A. B. Georgescu, G. Fabbris, M.-G. Han, Y. Zhu, J. W. Freeland, A. S. Disa, Y. Jia, M. P. M. Dean, F. J. Walker, S. Ismail-Beigi, C. H. Ahn, *Phys. Rev. Lett.* **2019**, 123, 117201.
- [26] G. van der Laan, B. T. Thole, *Phys. Rev. Lett.* **1988**, 60, 1977.
- [27] a)P. Carra, B. T. Thole, M. Altarelli, X. Wang, *Phys. Rev. Lett.* **1993**, 70, 694; b)B. T. Thole, P. Carra, F. Sette, G. van der Laan, *Phys. Rev. Lett.* **1992**, 68, 1943.
- [28] S. Agrestini, C. Y. Kuo, D. Mikhailova, K. Chen, P. Ohresser, T. W. Pi, H. Guo, A. C. Komarek, A. Tanaka, Z. Hu, L. H. Tjeng, *Phys. Rev. B* **2017**, 95, 245131.
- [29] L. Qiao, J. H. Jang, D. J. Singh, Z. Gai, H. Xiao, A. Mehta, R. K. Vasudevan, A. Tselev, Z. Feng, H. Zhou, S. Li, W. Prellier, X. Zu, Z. Liu, A. Borisevich, A. P. Baddorf, M. D. Biegalski, *Nano Lett.* **2015**, 15, 4677.
- [30] a)J. Matsuno, N. Ogawa, K. Yasuda, F. Kagawa, W. Koshibae, N. Nagaosa, Y. Tokura, M. Kawasaki, *Sci. Adv.* **2016**, 2, e1600304; b)A. Avsar, J. Y. Tan, T. Taychatanapat, J. Balakrishnan, G. K. W. Koon, Y. Yeo, J. Lahiri, A. Carvalho, A. S. Rodin, E. C. T. O'Farrell, G. Eda, A. H. Castro Neto, B. Özyilmaz, *Nat. Commun.* **2014**, 5, 4875.
- [31] a)A. Bedoya-Pinto, J.-R. Ji, A. K. Pandeya, P. Gargiani, M. Valvidares, P. Sessi, J. M. Taylor, F.

- Radu, K. Chang, S. S. P. Parkin, *Science* **2021**, 374, 616; b)C. Gong, L. Li, Z. Li, H. Ji, A. Stern, Y. Xia, T. Cao, W. Bao, C. Wang, Y. Wang, Z. Q. Qiu, R. J. Cava, S. G. Louie, J. Xia, X. Zhang, *Nature* **2017**, 546, 265; c)B. Huang, G. Clark, E. Navarro-Moratalla, D. R. Klein, R. Cheng, K. L. Seyler, D. Zhong, E. Schmidgall, M. A. McGuire, D. H. Cobden, W. Yao, D. Xiao, P. Jarillo-Herrero, X. Xu, *Nature* **2017**, 546, 270; d)J. L. Lado, J. Fernández-Rossier, *2D Mater.* **2017**, 4, 035002.
- [32] T. Kimura, Y. Tokura, *Annu. Rev. Mater. Sci.* **2000**, 30, 451.
- [33] S. G. Jeong, J. Y. Oh, L. Hao, J. Liu, W. S. Choi, *Adv. Funct. Mater.* **2023**, 33, 2301770.
- [34] A. Fert, N. Reyren, V. Cros, *Nat. Rev. Mater.* **2017**, 2, 17031.
- [35] a)L. Liu, Q. Qin, W. Lin, C. Li, Q. Xie, S. He, X. Shu, C. Zhou, Z. Lim, J. Yu, W. Lu, M. Li, X. Yan, S. J. Pennycook, J. Chen, *Nat. Nanotechnol.* **2019**, 14, 939; b)T. Nan, T. J. Anderson, J. Gibbons, K. Hwang, N. Campbell, H. Zhou, Y. Q. Dong, G. Y. Kim, D. F. Shao, T. R. Paudel, N. Reynolds, X. J. Wang, N. X. Sun, E. Y. Tsybal, S. Y. Choi, M. S. Rzechowski, Y. B. Kim, D. C. Ralph, C. B. Eom, *Proc. Natl. Acad. Sci. U. S. A.* **2019**, 116, 16186.
- [36] Y. Sun, A. Y. Abid, C. Tan, C. Ren, M. Li, N. Li, P. Chen, Y. Li, J. Zhang, X. Zhong, J. Wang, M. Liao, K. Liu, X. Bai, Y. Zhou, D. Yu, P. Gao, *Sci. Adv.* **2019**, 5, eaav4355.
- [37] a)X. Liu, S. Fang, Y. Fu, W. Ge, M. Kareev, J.-W. Kim, Y. Choi, E. Karapetrova, Q. Zhang, L. Gu, E.-S. Choi, F. Wen, J. H. Wilson, G. Fabbris, P. J. Ryan, J. W. Freeland, D. Haskel, W. Wu, J. H. Pixley, J. Chakhalian, *Phys. Rev. Lett.* **2021**, 127, 277204; b)J. Liu, X. Gao, K. Shi, M. Zhang, J. Wu, V. Ukleev, F. Radu, Y. Ji, Z. Deng, L. Wei, Y. Hong, S. Hu, W. Xiao, L. Li, Q. Zhang, Z. Wang, L. Wang, Y. Gan, K. Chen, Z. Liao, *Nano Lett.* **2024**, 24, 1351.
- [38] A. Barla, J. Nicolás, D. Cocco, S. M. Valvidares, J. Herrero-Martín, P. Gargiani, J. Moldes, C. Ruget, E. Pellegrin, S. Ferrer, *J. Synchrotron Radiat.* **2016**, 23, 1507.
- [39] a)P. Hohenberg, W. Kohn, *Phys. Rev.* **1964**, 136, B864; b)V. I. Anisimov, J. Zaanen, O. K. Andersen, *Phys. Rev. B* **1991**, 44, 943.
- [40] J. P. Perdew, K. Burke, M. Ernzerhof, *Phys. Rev. Lett.* **1996**, 77, 3865.

## Figures

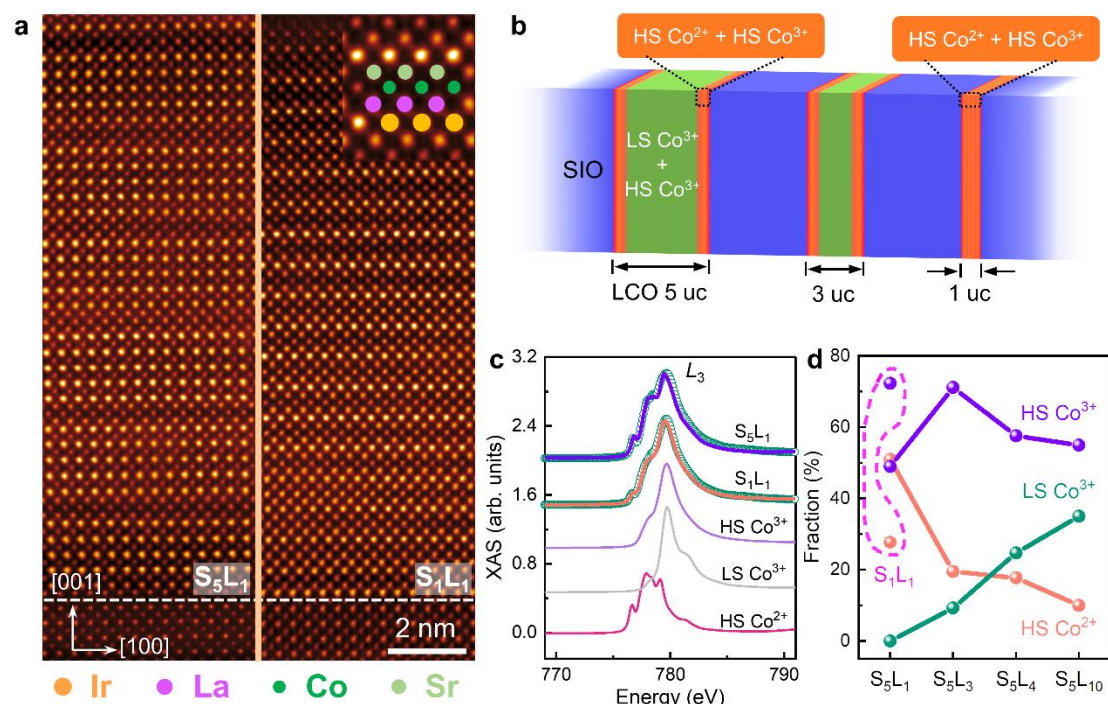


**Figure 1.** Evolution of nominal Co spin/electronic states. **a**, HAADF-STEM results of  $S_5L_1$  and  $S_1L_1$ . The inset is a zoom view of  $S_1L_1$  image. **b**, Schematic of spin state profile of Co ions. There are almost only HS  $Co^{2+}/Co^{3+}$  at interface, different from the bulk regime (green, dominated by HS/LS  $Co^{3+}$ ). **c**, Co- $L_3$  XAS fitting results of LCO monolayer SLs, where the feature of LS  $Co^{3+}$  (right shoulder) is absent. The spectra line-shape of  $S_5L_1$  and  $S_1L_1$  can be simulated by a linearly combination of only HS  $Co^{3+}$  and HS  $Co^{2+}$ , where 49% HS  $Co^{3+}$  and 51% HS  $Co^{2+}$  are for  $S_5L_1$ , and 72.3% HS  $Co^{3+}$  and 27.7% HS  $Co^{2+}$  are for  $S_1L_1$ . Reference HS  $Co^{3+}$ , LS  $Co^{3+}$ , and HS  $Co^{2+}$  XAS spectra are the experiment results of  $Sr_2Co_{0.5}Ir_{0.5}O_4$ ,  $NdCaCoO_4$  and  $CoO$ , respectively <sup>[19]</sup>. **d**, Fractions of HS  $Co^{3+}$ , LS  $Co^{3+}$  and HS  $Co^{2+}$  in superlattices for varied LCO thickness.

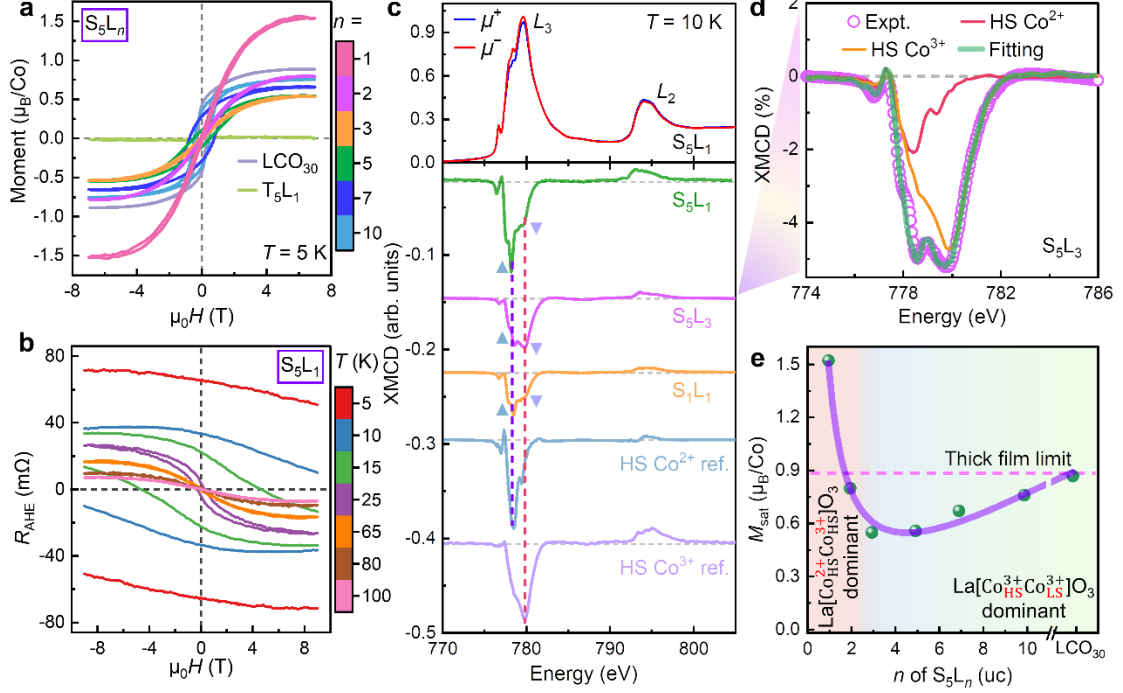


**Figure 2.** Survival and enhanced ferromagnetism as LCO down to monolayer. **a**, In-plane  $M$ - $H$  curves of  $S_5L_n$ ,  $T_5L_1$  and 30-uc  $\text{LaCoO}_3$  film ( $\text{LCO}_{30}$ ). **b**, AHE resistance ( $R_{\text{AHE}}$ ) hysteresis of  $S_5L_1$ . See **Experimental Section/Methods** for measurement details. **c**, Co- $L_{2,3}$  XMCD results at 10 K with applied field (6T) perpendicular to sample plane, where the reference spectra of HS  $\text{Co}^{3+}$  and HS  $\text{Co}^{2+}$  are the experimental XMCD results of  $\text{Sr}_2\text{CoIrO}_6$  [17c] and  $\text{CoO}$ , respectively. The signal magnitudes of XMCD, defined as a percentage of the maximum of corresponding Co- $L_3$  edge, were 8.9% for  $S_5L_1$ , 4.9% for  $S_5L_3$  and 4.5% for  $S_1L_1$ . By linearly combining the reference spectra of HS  $\text{Co}^{3+}$  and HS  $\text{Co}^{2+}$ , the XMCD of  $S_5L_3$  is almost perfectly reproduced in **d**. **e**, Evolution of Co saturated moment ( $M_{\text{sat}}$ ) with LCO thickness at 5 K.

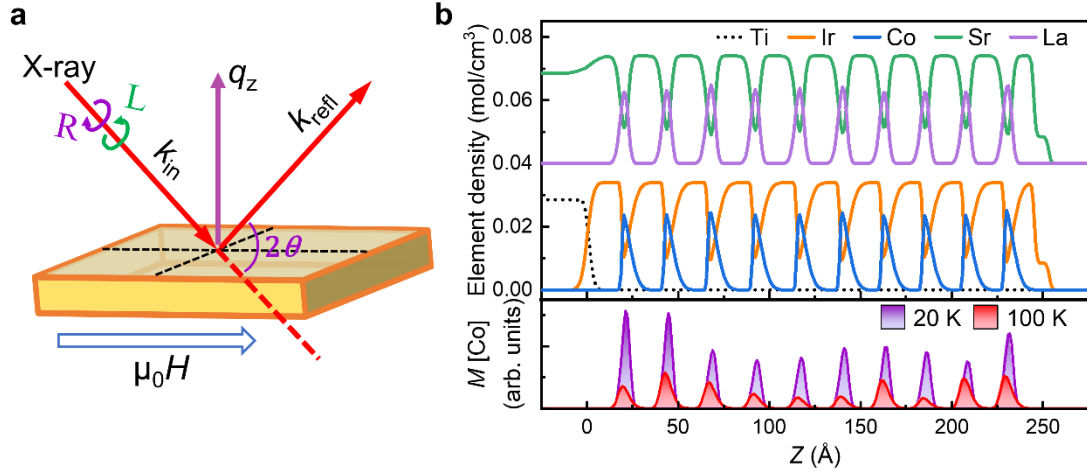


**Figure 3.** Ferromagnetism beyond 100 K in LCO monolayer. **a**, Experimental set-up sketch of RSXR measurements, where a 0.6 T magnetic field was applied in-plane during the measurement. **b**, Magnetic and element profiles in  $S_5L_1$  at 20 K and 100 K along the [001] direction ( $Z$ ), where the terminated LCO was capped by additional 3 uc SIO for avoiding degradation. For clarity, the element density of A-site ions, including La and Sr, is offset vertically by 0.04.

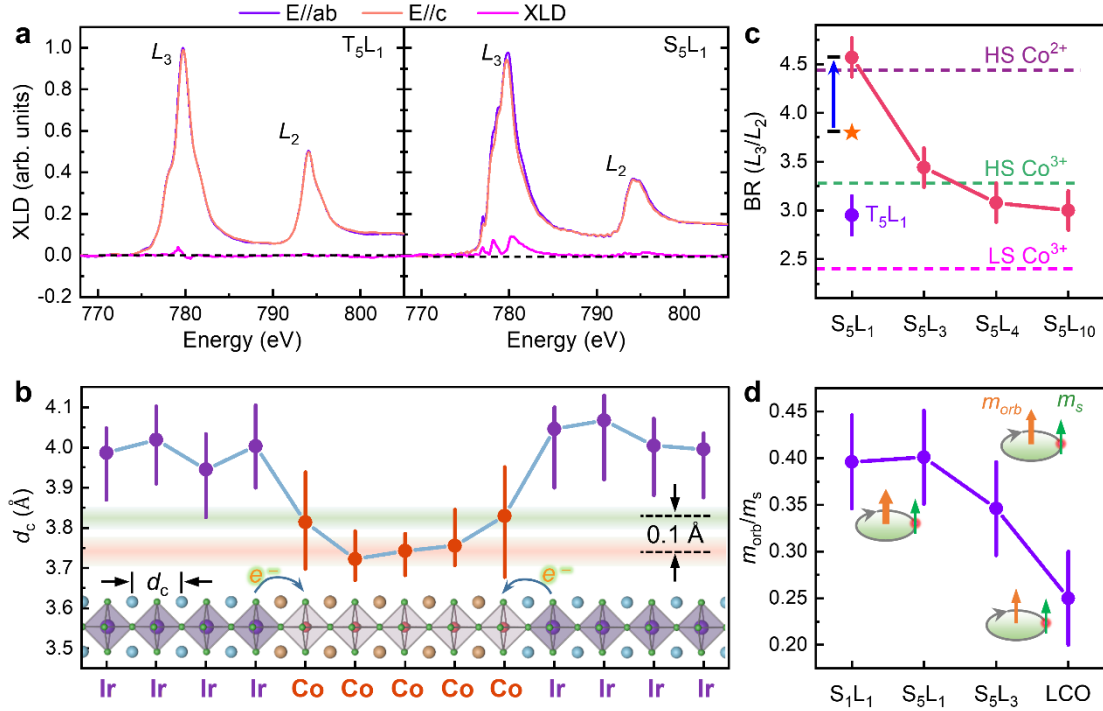


**Figure 4.** Anomalous orbital reconstruction and enhanced SOC. **a**, XLD results at Co- $L_{2,3}$  edge, which is defined as  $I_{E//ab} - I_{E//c}$ . **b**, Increased  $c$ -axis length ( $d_c$ ) near interface in  $S_5L_5$ , which is characterized by the distance between two adjacent A-sites as illustrated by the inset. These results were obtained statistically from a  $22 \text{ uc} \times 22 \text{ uc}$  cross-section region of the HAADF image. **c**, Branching ratio ( $\text{BR} = L_3/L_2$ ) extracted from Co- $L_{2,3}$  XAS, where the reference levels (dashed line) are derived from experimental spectra <sup>[19]</sup>. The orange five-pointed star denotes the calculated weighted average  $\text{BR}^*$  based on the reference levels. **d**, Evolution of  $m_{\text{orb}}/m_s$ , where the data of LCO is extracted and processed from ref. <sup>[1a]</sup>. The error bars of BR and  $m_{\text{orb}}/m_s$  are from the final state effects of the core level SOC and core-valence exchange interactions (multiplet effects) of Co ions.

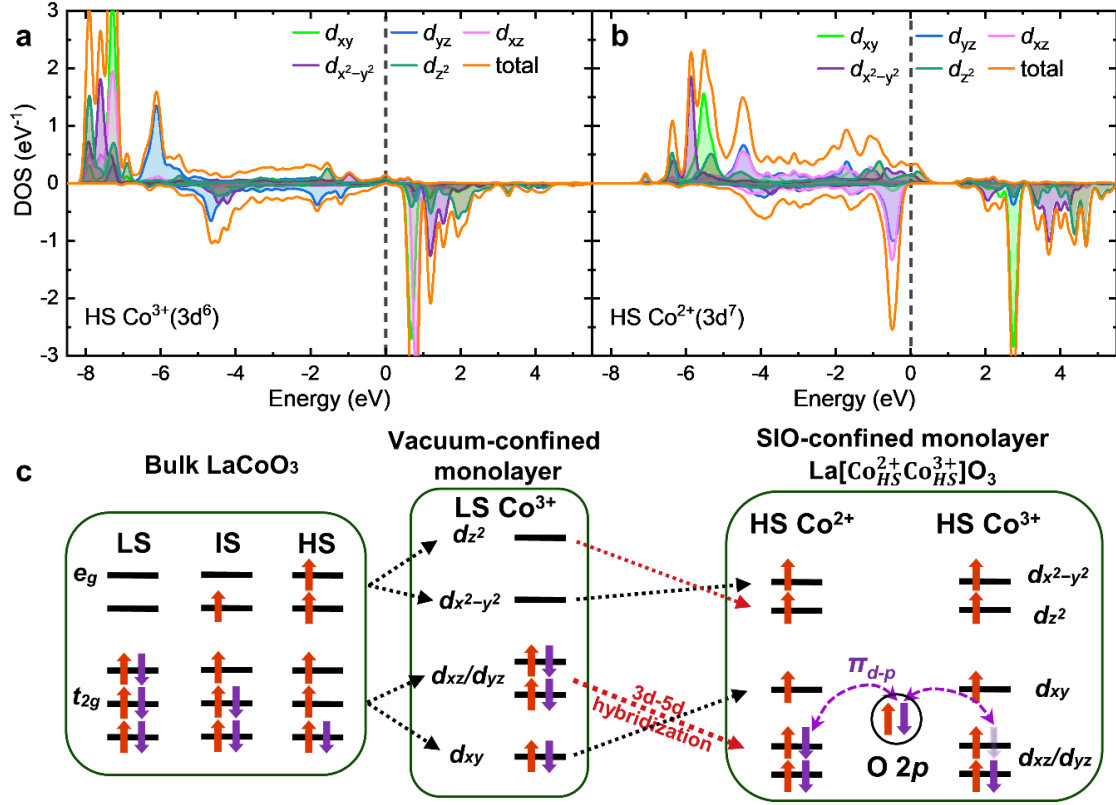


**Figure 5.** Theoretical calculations using DFT+U. DOS of HS Co<sup>3+</sup> and HS Co<sup>2+</sup> are shown in **a** and **b**, respectively. **c**, Schematic of the energy-level distribution of Co3d in LCO under different cases. Left panel are for bulk LCO, where LS, IS, and HS configurations are shown here. Vacuum-confined LCO monolayer (middle panel) possesses a LS configuration due to the confinement effect. Fully HS state with the coexistence of Co<sup>2+</sup> and Co<sup>3+</sup> is shown in right panel. Double exchange interaction between HS Co<sup>2+</sup> and HS Co<sup>3+</sup> is mediated by t<sub>2g</sub> (d<sub>xz</sub>/d<sub>yz</sub>) electron via Co-O π<sub>d-p</sub> bond, which causes ferromagnetism in LCO monolayer.







